Laboratory study of nitrate photolysis in Antarctic snow. II. Isotopic effects and wavelength dependence

Tesfaye A. Berhanu, Carl Meusinger, Joseph Erbland, Rémy Jost, S. K. Bhattacharya, Matthew S. Johnson, Joël Savarino

RESEARCH ARTICLE | JUNE 24 2014

Laboratory study of nitrate photolysis in Antarctic snow. II. Isotopic effects and wavelength dependence

Tesfaye A. Berhanu; Carl Meusinger; Joseph Erbland; Rémy Jost; S. K. Bhattacharya; Matthew S. Johnson; Joël Savarino

J. Chem. Phys. 140, 244306 (2014)
https://doi.org/10.1063/1.4882899

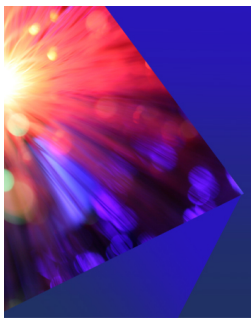

Laboratory study of nitrate photolysis in Antarctic snow. II. Isotopic effects and wavelength dependence

Tesfaye A. Berhanu,[1,2] Carl Meusinger,[3] Joseph Erbland,[1,2] Rémy Jost,[4]
S. K. Bhattacharya,[5] Matthew S. Johnson,[3] and Joël Savarino[1,2]
[1]*Laboratoire de Glaciologie et Géophysique de l'Environnement, CNRS, F-38041 Grenoble, France*
[2]*Univ. Grenoble Alpes, LGGE, F-38041 Grenoble, France*
[3]*Copenhagen Center for Atmospheric Research (CCAR), Department of Chemistry, University of Copenhagen, Copenhagen, Denmark*
[4]*Laboratoire de Interdisciplinaire de Physique (LIPHY) Univ. de Grenoble, Grenoble, France*
[5]*Research Center for Environmental Changes, Academia Sinica, Nangang, Taipei 115, Taiwan*

(Received 18 December 2013; accepted 25 March 2014; published online 24 June 2014)

Atmospheric nitrate is preserved in Antarctic snow firn and ice. However, at low snow accumulation sites, post-depositional processes induced by sunlight obscure its interpretation. The goal of these studies (see also Paper I by Meusinger *et al.* ["Laboratory study of nitrate photolysis in Antarctic snow. I. Observed quantum yield, domain of photolysis, and secondary chemistry," J. Chem. Phys. **140**, 244305 (2014)]) is to characterize nitrate photochemistry and improve the interpretation of the nitrate ice core record. Naturally occurring stable isotopes in nitrate (^{15}N, ^{17}O, and ^{18}O) provide additional information concerning post-depositional processes. Here, we present results from studies of the wavelength-dependent isotope effects from photolysis of nitrate in a matrix of natural snow. Snow from Dome C, Antarctica was irradiated in selected wavelength regions using a Xe UV lamp and filters. The irradiated snow was sampled and analyzed for nitrate concentration and isotopic composition (δ^{15}N, δ^{18}O, and Δ^{17}O). From these measurements an average photolytic isotopic fractionation of $^{15}\varepsilon = (-15 \pm 1.2)‰$ was found for broadband Xe lamp photolysis. These results are due in part to excitation of the intense absorption band of nitrate around 200 nm in addition to the weaker band centered at 305 nm followed by photodissociation. An experiment with a filter blocking wavelengths shorter than 320 nm, approximating the actinic flux spectrum at Dome C, yielded a photolytic isotopic fractionation of $^{15}\varepsilon = (-47.9 \pm 6.8)‰$, in good agreement with fractionations determined by previous studies for the East Antarctic Plateau which range from −40 to −74.3‰. We describe a new semi-empirical zero point energy shift model used to derive the absorption cross sections of $^{14}NO_3^-$ and $^{15}NO_3^-$ in snow at a chosen temperature. The nitrogen isotopic fractionations obtained by applying this model under the experimental temperature as well as considering the shift in width and center well reproduced the values obtained in the laboratory study. These cross sections can be used in isotopic models to reproduce the stable isotopic composition of nitrate found in Antarctic snow profiles. [http://dx.doi.org/10.1063/1.4882899]

I. INTRODUCTION

Nitrate is the end product of atmospheric NO_x ($NO + NO_2$) oxidation and the NO_x cycle is strongly coupled with OH and O_3 chemistry in the atmosphere. The oxygen isotope ratios in nitrate provide information about the oxidation pathways of nitrate formation, and incorporate the anomalous isotopic composition of ozone.[1,2] In polar regions, nitrate is one of the most abundant anions in snow,[3] and has a significant potential for documenting past climate change including the oxidation capacity of the atmosphere.[4] In addition, as nitrogen isotopes are conserved from source to sink during nitrate formation, they are used as tracers to identify the sources of NO_x.[5]

The stable isotope ratios ($n(^{18}O)/n(^{16}O)$, $n(^{17}O)/n(^{16}O)$, and $n(^{15}N)/n(^{14}N)$, where n is the amount of each isotope) of nitrate are expressed as δ-values (δ^{17}O, δ^{18}O, and Δ^{17}O) where $\delta = (R_{spl}/R_{ref})$-1 is the ratio of R of the sample (R_{spl}) and reference (R_{ref}) with references being atmospheric nitrogen and Vienna Standard Mean Ocean Water (VSMOW) for N and O respectively. The ^{17}O-excess is expressed by the linear relation $\Delta^{17}O = \delta^{17}O - 0.52\times\delta^{18}O$. The stable isotope ratios of nitrate in snow have been used to investigate the sources and formation pathways of snow nitrate in polar regions.[2,6] However, the large loss of snow nitrate[7,8] and simultaneous isotopic fractionation, especially at sites with low snow accumulation rates[9,10] indicate that post-depositional processes including evaporation/sublimation and UV photolysis significantly modify the original nitrate mass and isotopic signal. This conclusion is supported by the elevated atmospheric NO_X levels above the snowpack, and by the profiles of nitrate concentration and stable isotope ratios in snow at these locations[8–12] described below.

Multiple field studies in both the Arctic and Antarctic show elevated NO_x levels in association with sunlight and the

snowpack has been shown to be the source[13–15] although the production mechanism is not well understood.[16]

By analogy with reactions known to occur in the aqueous phase, photolysis of nitrate in ice is believed to involve the following elementary reactions:[17–19]

$$NO_3^- + h\nu \rightarrow NO_2 + O^-, \quad \text{(R1)}$$

$$NO_3^- + h\nu \rightarrow NO_2^- + O(^3P), \quad \text{(R2)}$$

$$NO_2^- + h\nu \rightarrow NO + O^-, \quad \text{(R3)}$$

$$NO_2^- + OH \rightarrow NO_2 + OH^-. \quad \text{(R4)}$$

NO_2 is the primary photoproduct of nitrate photolysis;[20] (R1) is 8–9 times faster than (R2).[16] Nitrite produced via (R2) may be photolyzed producing NO (R3) or it may react with a hydroxyl radical to produce NO_2 (R4). It has also been suggested that NO_X photoproducts react with the remaining snow nitrate, thus amplifying the denitrification of the snow with its own isotopic fractionation.[21] Ultimately, the products from nitrate photolysis are emitted to the atmosphere where they influence O_3 and HO_x chemistry and have a significant impact on the composition of the boundary layer, further complicating the interpretation of information archived in deep ice cores.[12,16,17,22–26]

A series of studies have used stable isotope distributions to investigate nitrate and nitrate-related photochemistry in snow. Blunier *et al.*[10] investigated nitrate mass loss and nitrogen isotopic fractionation ($^{15}\varepsilon$) in artificial snow that was doped with $NaNO_3$ and irradiated with a Xe UV lamp. As the isotopic fractionations of this experimental study did not agree with their field observations, the authors ruled out photolysis as the main post depositional loss mechanism for nitrate. However, in a later study by Frey *et al.*,[9] it was shown that the isotopic fractionation obtained by Blunier *et al.*[10] was not a true representation of the field conditions and the observed isotope effects were caused by the emission spectrum of the Xe lamp in the experiments and the lack of removal of photoproducts. Based on field measurements, Frey *et al.*[9] determined an apparent isotopic fractionation ($^{15}\varepsilon_{app}$) and proposed that photolysis is the main mechanism responsible for the observed fractionation of stable isotopes of nitrate. In their theoretical analysis, the authors applied a simple zero point energy shift (ΔZPE-shift) model[27] and derived an isotopic fractionation in the wavelength region of interest (−48‰) which is close to the values observed in the field ((−60 ± 15)‰[9] and (−54 ± 10)‰[10]). More recently Erbland *et al.*[28] derived an average apparent nitrogen isotopic fractionation of (−59 ± 10)‰ for the East Antarctic Plateau. However, the variability of field conditions limited the accuracy of the resulting isotopic fractionations associated with processes within the snowpack, including the wavelength dependency for the photolysis effect.[9,28] Additionally, the ΔZPE-shift approach[9] used previously to obtain $\sigma(^{15}NO_3^-)$ from $\sigma(^{14}NO_3^-)$ and determine the photolytic isotopic fractionation involves a number of approximations[29] and should be revised for two reasons: (a) because it assumes that the shape and amplitude of the cross section are unchanged upon N (or O) isotope substitution and (b) because the value of the ΔZPE-shift of −44.8 cm^{-1} does not account the contributions from vibrational anharmonicities or the ZPE shift in the excited state. These two points are detailed in Appendix B. The absorption cross section of $^{15}NO_3^-$ can be better estimated using detailed knowledge of the different parameters modified during isotopic substitution and such a theoretical approach has recently been presented for simple molecules by Jost and co-workers.[30,31] The model considers changes in four fundamental parameters (amplitude, center, width, and symmetry) associated with isotopic substitution (Appendix B). The aforementioned limitations of the existing studies demonstrate the need for further laboratory studies with improved experimental design and for a more thorough theoretical treatment.

Paper I by Meusinger *et al.*[32] focuses on the physical chemistry of photolysis of nitrate in snow, and specifically on the quantum yield for photodissociation of nitrate in its different domains in natural snow. The main goal of the present paper is to understand the effect of photolysis and its photoproducts on the stable isotope enrichments of nitrate in an experimental setup that controls key parameters such as temperature, excitation spectrum, isotopic exchange, and product reactivity and removal.

In this paper, we investigate the fractionation of oxygen and nitrogen stable isotopes in Dome C snow nitrate in response to photolysis in different UV wavelength regions. We also test if isotopic exchange and/or chemical reaction between NO_x photoproducts and the snow nitrate is present. We discuss these results using an improved version of the zero point energy shift model developed by Frey *et al.*[9] In addition, we re-evaluate previous studies in the light of our results and model, and discuss directions for future work.

II. METHODS

A. Experimental setup and sample handling

The detailed experimental setup is described in Paper I[32] and will only be summarized here. After a strong wind event, wind-blown snow from the vicinity of the Concordia station, Antarctica (75°S 06′ and 124°E 33′) was collected and homogenized on December 6th, 2011 and transported to France. Nitrate concentrations in the snow sample at the time of collection (29 nmol g^{-1}) and before photolysis experiments (27 nmol g^{-1}) agree to within the analytical uncertainty (<3%),[9] demonstrating that temperature and environmental variations had negligible effect on the snow nitrate and indicating that the majority of nitrate is probably not physically adsorbed in the form of HNO_3 on the surface of the grain crystals.

For each experiment a sample of 110–120 g of snow was homogenized by gentle crushing into loose grains and transferred into a cylindrical Pyrex glass cell of 30 cm length and 6 cm internal diameter (Figure 1). A Teflon sleeve was used to line the snow column inside the cell. The sleeve helped to prevent the snow sample from sticking to the glass cell and eased sampling after the experiments. Two end caps with suprasil UV windows (L.O.T. Oriel) are clamped to the main section

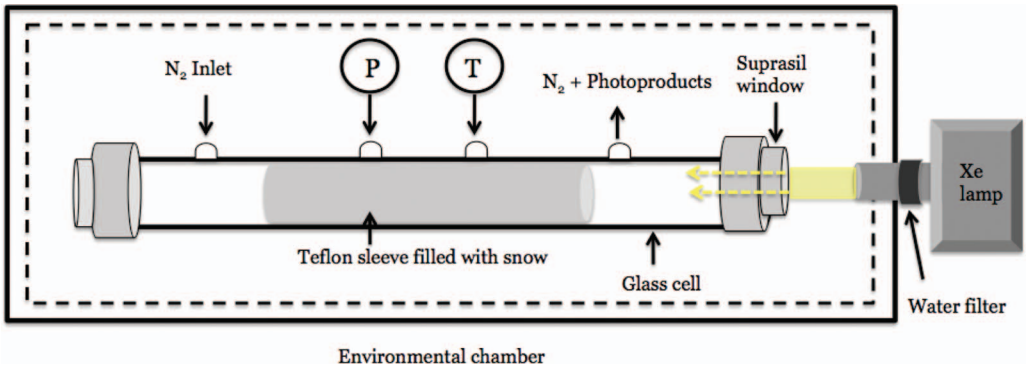

FIG. 1. Schematic of the experimental setup used in this study. Natural snow was filled in the glass cell (total length of about 30 cm and internal diameter of 6 cm) with temperature (T) and pressure (P) probes and irradiated with a Xe lamp. A flow of nitrogen (relative humidity 100%) was used to remove the photoproducts. The water filter at the front of the lamp enabled removal of the infrared[52] part of the incoming light.

of the cell. The main section has four ports on the upper side: two of these were used as inlets and outlets for water saturated N_2 flow and two others to monitor temperature and pressure inside the cell during the experiment.

For photolysis experiments, a Xe lamp (L.O.T. Oriel, 300 Watt) with the spectral range of 200–900 nm was used as light source with a water filter at the front to minimize the IR heat flux into the snow. UV filters with different cut-off wavelengths were attached at the front of the lamp (LOT Oriel, Andover Corporation) as required.

The nitrate absorption cross section has two main peaks in the UV region, at about 200 and 305 nm. The former is 3 orders of magnitude larger than the latter.[33] In order to study the wavelength dependence of nitrate photolysis in the UV region the Xe lamp output UV flux was modified with long-pass UV filters with cut off (50% level reduction) wavelengths at 280 nm, 305 nm, and 320 nm.[32] The experimental conditions are detailed in Table I.

At the end of each experiment, the snow was slowly pushed out of the Teflon sleeve and sampled in 1–2 cm slices with a scalpel. Each sub sample (5–10 g) was homogenized and divided into two parts, weighed, and sealed to measure the concentration and isotopic composition of the snow nitrate.

TABLE I. Experimental conditions for the experiments. In each case a flow rate of 2.2 l min^{-1} is used to flush away the NO_x by-products. Experiments are performed at −30 °C with natural snow from Dome C.

No.	Case	Duration, h
1	Dark experiment	139.5
2[a]	Temperature cycle	160.5
3	NO_2 ^{15}N-exchange in dark	120.0
4	NO ^{15}N-exchange in dark	162.0
5	NO_2 reactivity in UV-light/air-zero	161.0
6	No filter	20.3
7	No filter	162.8
8	280 nm filter	164.0
9	305 nm filter	187.2
10	320 nm filter	283.2

[a]Experiment conducted with a variable temperature, ranging from −28 °C to −38 °C diurnally.

B. Control experiments

Two initial control experiments were conducted in the dark to determine whether non-photolytic processes with the potential to induce nitrate mass loss and/or isotopic fractionation were active. In the first reference experiment (case 1: baseline), the snow was exposed to a flow of N_2 saturated with water vapor (2 l min^{-1}) for 7 days in the dark at a constant temperature of −30 °C. In the second similar experiment (case 2: temperature cycle), the temperature of the system was varied between −28 °C and −38 °C during 7 days to simulate the summer time diurnal temperature variation observed at Dome C. This experiment was designed to test nitrate mass loss by physical release only.

Isotopic exchange and/or chemical reaction between NO_x photoproducts and snow nitrate has been debated recently as a possible cause of isotopic fractionation.[34] To test this hypothesis, we conducted a series of separate experiments. In experiment 3 (case 3: NO_2 ^{15}N-exchange test in the dark), ^{15}N-enriched NO_2 ($\delta^{15}N \approx 180‰$) generated from the thermal decomposition of USGS-32[35] (KNO_3 salt) and diluted in He flowed at a concentration of tens of nmol mol^{-1} (corresponding to recent NO_x measurements in the snowpack at Dome C[36]) through the snow in the dark for 7 days with N_2 carrier gas. A separate similar experiment was conducted with NO mixed in He (mole fraction = 10 ppb and $\delta^{15}N$ = −40‰) (case 4: NO ^{15}N-exchange test). A photoproduct reaction test (case 5) was conducted where air-zero (made using ultra high purity N_2 and O_2 tanks) mixed with NO_2 in He (in identical ratios as in experiment #3) flows through a snow column exposed to a Xe UV-lamp equipped with a 320 nm UV-filter. The air-zero in this case was used as a bath gas to remove any O-atoms produced by the photodissociation of NO_2.

C. Sample analysis

The nitrate concentration in the snow samples was analyzed using an Ion Chromatography system (850 Professional IC, Metrohm). The stable isotope ratios of nitrate were measured on a Thermo Finnigan™ MAT 253 Isotope Ratio Mass Spectrometer equipped with a GasBench II™ and coupled to

a specially designed nitrate interface.[37] Briefly, denitrifying bacteria *Pseudomonas Aureofaciens* convert NO_3^- to N_2O in anaerobic conditions.[38,39] The N_2O is thermally decomposed on a gold surface heated to 900 °C, producing O_2 and N_2 which is separated by gas chromatography[40] and injected into the mass spectrometer for the dual O and N analysis.[37] An algorithm was used to calibrate the results to account for blank effects and isotopic exchange with the bacterial matrix that could arise due to the small sample size. To correct for isotope effects associated with sample analysis we have included certified standards of USGS-32, USGS-34, and USGS-35[35,41] which are treated in the exact same way as the samples and prepared in the same matrix as the samples (MQ water),[37] at a range of concentrations (20–100 nmol). This enabled us to perform a nonlinear calibration for some of the samples containing less than 50 nmol of material. Using this algorithm the overall accuracy of the method is determined from the standard deviations of the residuals of the linear regression between the measured and expected isotopic values of the references. For the samples analyzed in this study, the associated average uncertainties are 2.25‰, 0.6‰, and 0.6‰ for $\delta^{18}O$, $\Delta^{17}O$, and $\delta^{15}N$, respectively. The larger uncertainties observed in these measurements relative to typical values are due to samples smaller than the optimal 100 nmol range.

D. Data reduction

The photolysis rate constants for a given isotopic species (e.g., $^{14}NO_3^-$) is given by

$$J^{14} = \int \phi(\lambda, T)\,\sigma(\lambda, T)\,I(\lambda)\,d\lambda, \tag{1}$$

where $\sigma(\lambda)$ is the absorption cross section (in this example, $^{14}NO_3^-$), $\phi(\lambda)$ is the quantum yield and $I(\lambda)$ is the measured actinic flux of the filtered UV Xe lamp in appropriate units (Figure 2(a)). The photolysis rates $J(^{14}NO_3^-)$ calculated using Eq. (1) as a function of wavelength for the different filters are shown in Figure 2(b).

The isotopic fractionation ($^{15}\varepsilon$) associated with the unidirectional loss of nitrate during photolysis is determined using the Rayleigh equation:[9,10]

$$\frac{R}{R_0} = \frac{\delta + 1}{\delta_0 + 1} = f^{\varepsilon}, \tag{2}$$

where R_0 and R are the isotope ratios n(^{15}N)/n(^{14}N) in nitrate before and after photolysis. ($f = C/C_0$) denotes the remaining fraction of nitrate in snow at some reaction time, with the initial and time-dependent concentrations given by C_0 and C, and enrichments δ_0 and δ. From Eq. (2) the following relationship is obtained:

$$\ln(\delta + 1) = \varepsilon \ln(f) + \ln(\delta_0 + 1). \tag{3}$$

Plotting $\ln(\delta+1)$ versus $\ln(f)$ gives the isotopic fractionation ε as the slope. (Note that ε is related to the fractionation factor α by $\varepsilon = \alpha - 1$.) The (1σ) uncertainty in ε is based on the propagation of the error in the isotope ratios, as in Frey *et al.*[9] based on Taylor.[42]

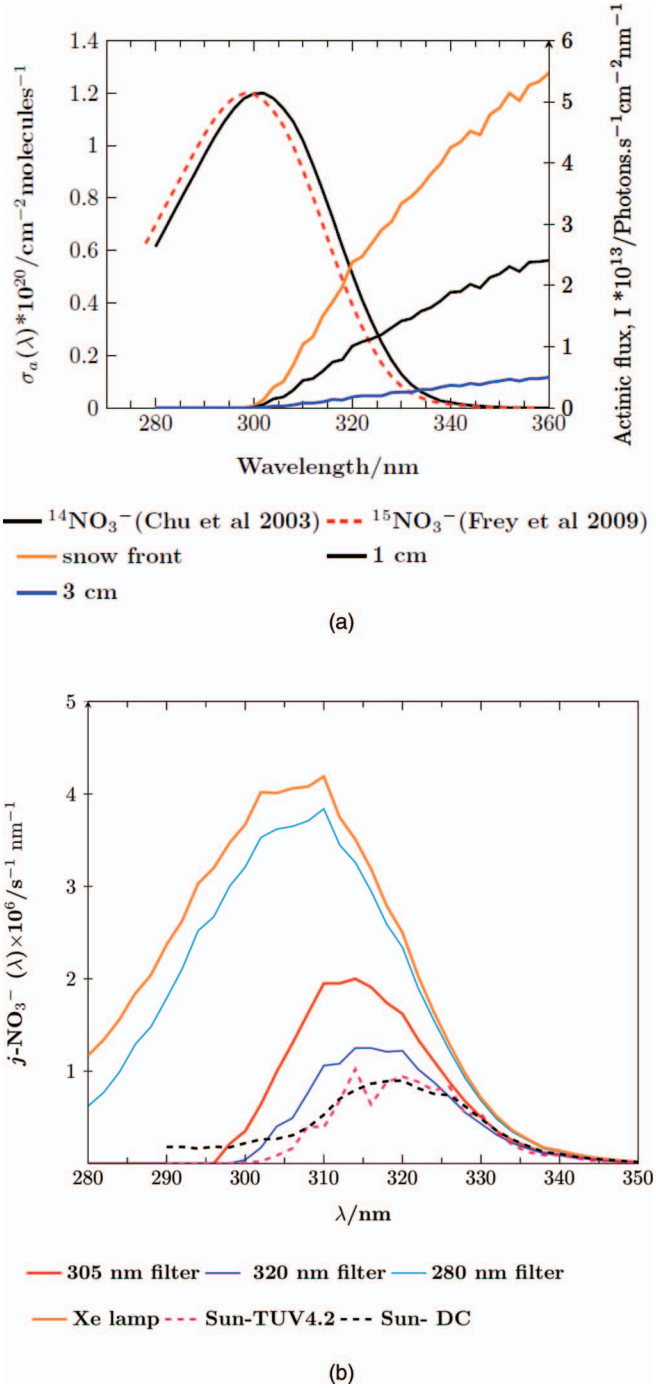

FIG. 2. (a) The absorption cross-section of $^{14}NO_3^-$ measured in the liquid phase[43] and $^{15}NO_3^-$ taken from the ZPE-shift model by Frey *et al.*[9] as a function of wavelength shown on the left y-axis as well as the actinic flux (right y-axis) of the filtered lamp spectra (using the 320 nm filter) at the front of the snow (depth = 0 cm) and at depths of 1 cm and 3 cm. Note that the ZPE-shift was made artificially large (≈2 nm) for visual purpose but the actual the absorption cross-sections of nitrate isotopologues nearly overlap (≈0.5 nm). (b). Photolysis rates j(λ) of $^{14}NO_3^-$ determined for each UV filter calculated from measured irradiance of the lamp in the presence of the different filters[32] and using the absorption cross section of nitrate determined by Chu and Anastasio.[43] The solar photolysis rate of nitrate is determined using the solar actinic flux at Dome C derived using TUV model 4.4 for January 15, 2004, with 297 DU ozone column and with an albedo of 0.9 (as used in Frey *et al.*[9]). Sun-DC is derived from the solar irradiance measured at Dome C on January 8th, 2013 at 2 pm local time.[57] The flat line at λ < 300 nm in the Sun-DC line from an irradiance measurement at Dome C is associated with the instrumental noise.

The isotopic fractionation is also determined theoretically using the equation:

$$\varepsilon = \frac{J^{15}}{J^{14}} - 1, \tag{4}$$

where J^{15} and J^{14} are the photolytic rate constants for the heavy ($^{15}NO_3^-$) and the light ($^{14}NO_3^-$) isotopologues, respectively, determined using Eq. (1) from their corresponding absorption cross sections of $\sigma^{15}(\lambda)$ and $\sigma^{14}(\lambda)$ (Fig. 2(a)) and the spectral actinic flux $I(\lambda)$. In this study, we have measured the actinic flux of the Xe lamp and the lamp combined with UV filters at different depths.[32] The absorption cross section of $^{14}NO_3^-$ was obtained from Chu *et al.*[43] and the absorption cross section of $^{15}NO_3^-$ was taken from Frey *et al.*[9] Note that since we have assumed the quantum yield ($\phi(\lambda)$) to be independent of wavelength and to be similar for $^{14}NO_3^-$ and $^{15}NO_3^-$, there is no need to know its exact value to determine the isotopic fractionation. The calculated isotopic fractionations ($^{15}\varepsilon_{pho}$) were then directly compared with the values obtained from the snow experiments.

III. RESULTS

A. Control experiments

Figures 3, 7, and 8 clearly show that in the absence of UV light the snow remains unchanged (no change in the specific surface area of the snow was observed, see Paper I[32]), and the nitrate concentration and its isotopic composition remain unaltered. These observations (cases 1 and 2) confirm that the physical losses (e.g., desorption) are negligible and do not induce isotopic fractionation in the current experimental setup. This is also an indication that nitrate is probably not located on the surface of the snow crystal in the form of adsorbed HNO_3. Isotopic exchange between the photoproducts NO or NO_2 and the snow nitrate can also be discounted; it is not observed in the dark (cases 3 and 4) or with light (case 5). The same conclusion can be drawn for possible chemistry between the NO_x photoproducts and the snow nitrate. There is no indication that NO or NO_2 react with snow nitrate and induce a significant modification of its concentration or isotopic profiles (see Figure 8). These observations clearly indicate that the modifications observed in Figure 3 are only the result of snow nitrate photolysis.

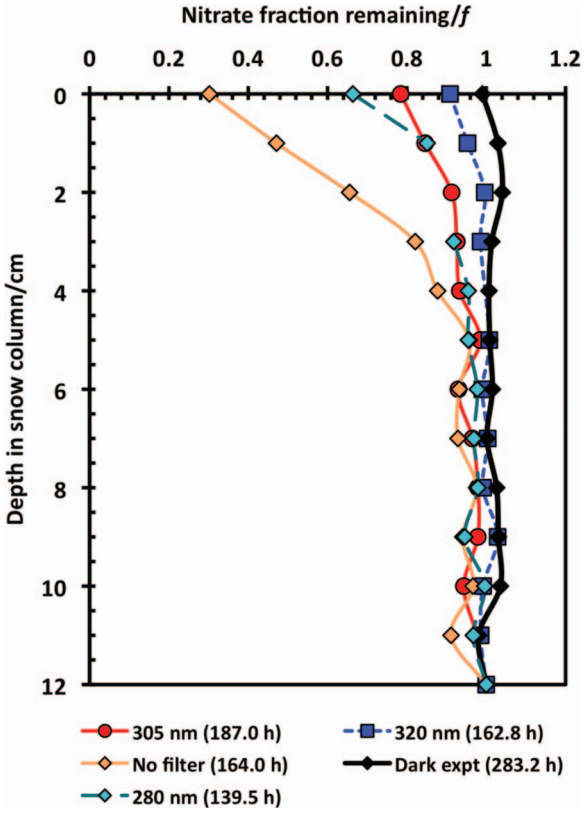

FIG. 3. Nitrate concentration profile (fraction of nitrate remaining, f) versus depth in the snow column plotted for the experiments conducted using different filters."0" represents the side of the snow column closest to the lamp.

B. Nitrate concentration measurements

Results for the change in nitrate concentration due to UV-irradiation of Antarctic snow by a Xe lamp with optical filters is discussed in Paper I;[32] here we will summarize the relevant conclusions. The measured nitrate concentration and the calculated nitrate fraction remaining (f) at the end of each experiments are given in Figures 9 and 3, respectively. The experiment conducted without an UV filter (case 7) shows about 70% nitrate loss for the front sample, with decreasing loss with depth in the snow column. The experiments using the 280 nm and 305 nm filters also showed varying losses depending on the duration of UV exposure and the fraction of UV light around 305 nm that was attenuated by the filters. The 320 nm filter experiment showed only a small loss after 12 days of irradiation.

C. Isotopic measurements

1. $\delta^{15}N$ measurements

Figure 4 shows the $\delta^{15}N$ profile for the experiments conducted using different UV-filters. For each experiment the $\delta^{15}N$ increases in the first 4–5 cm from the initial value of −3.8‰, concomitant with the nitrate mass loss. However, the increase in $\delta^{15}N$ corresponds to the type of UV filter used, with higher $\delta^{15}N$ for the no-filter experiment and lower values for the 320 nm filter.

2. $\delta^{18}O$ and $\Delta^{17}O$ measurements

The determination of the oxygen isotopes was affected by the small sample sizes and the results are associated with large error bars. In contrast to the observed clear trend in the $\delta^{15}N$ measurements, $\delta^{18}O$ and $\Delta^{17}O$ showed no systematic variations, as shown in Appendix A (Figures 10 and 11). Hence, quantitative information could not be obtained from these measurements but it should be noted that the general trend observed in these measurements are not in contradiction with the field observations.

3. Depth dependence of the isotopic fractionation

As observed in the concentration and isotope profile plots, no measurement shows a significant change below

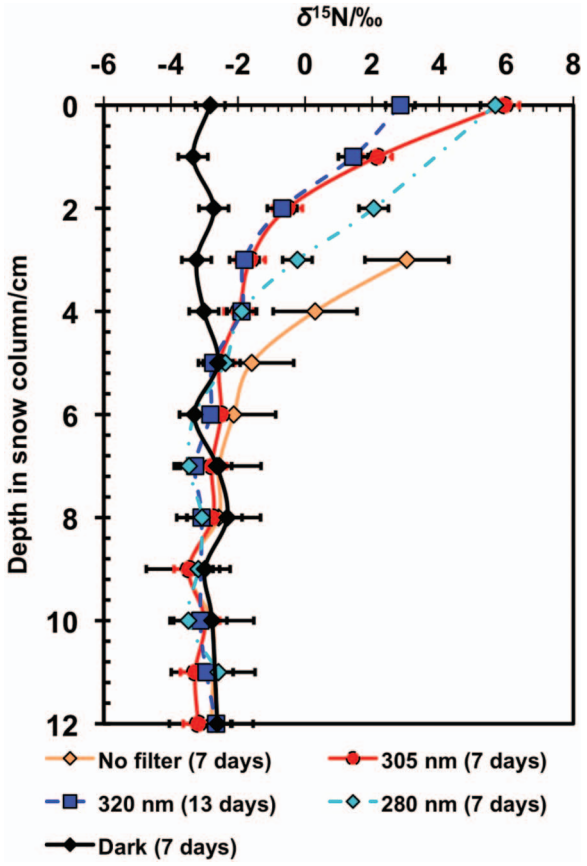

FIG. 4. The δ^{15}N profile with depth in the snow column for the experiments conducted using different filters. The δ^{15}N values for the top two samples of the no filter experiment could not be measured due to the intense loss of nitrate leading to a nitrate concentration (6 nmol ml^{-1}) below the analysis limit.

7 cm. This is due to the scattering of light within the first few centimeters of depth. In this sense the laboratory conditions are different from the field conditions, as the boundary conditions are not semi-infinite[44] (see also Meusinger *et al.*[32]). Hence, we have considered only the top 7 cm in evaluating the depth dependence of the isotopic fractionations.

Based on the irradiance measurements at every 1 cm depth starting from the front side (close to the lamp[32]), we have observed a uniform attenuation of the incoming light flux by the snow layers. The nitrogen isotopic fractionations were

TABLE II. Calculated isotopic fractionation constants at different depths in the snow column for the 305 nm and 320 nm filter experiments.

Depth/cm	305 nm filter $^{15}\varepsilon$/‰	320 nm filter $^{15}\varepsilon$/‰
0	−36.75	−42.80
1	−36.86	−42.95
2	−36.97	−43.10
3	−37.08	−43.25
4	−37.18	−43.39
5	−37.28	−43.53
6	−37.43	−43.74
7	−37.70	−44.12
	(−38.6 ± 2.8)[a]	(−47.9 ± 6.8)[a]

[a]Experimentally observed $^{15}\varepsilon$ values for the two filters.

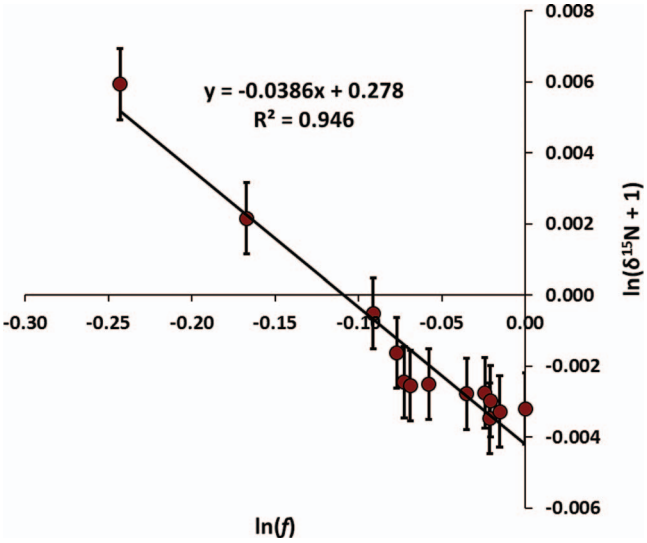

FIG. 5. A typical Rayleigh plot for the experiment conducted using 305 nm UV-filter for 187.2 h. An isotopic fractionation of (−38.6 ± 2.2)‰ was obtained for this experiment.

calculated using these measured irradiances at every 1 cm and applying Eq. (1). Results for experiments 4 and 5 (305 nm and 320 nm UV filters) are presented in Table II. Accordingly, for the 305 nm filter, we have calculated a fractionation constant of −33.5‰ at the top of the snow column, decreasing to −34.5‰ at 7 cm depth. Similarly, for the 320 nm filter, a fractionation constant ranging from −39.3‰ to −40.7‰ was calculated. The obtained results are not significantly different for a given filter at different depths which is expected based on the uniformly attenuated light flux with depth.

4. Nitrogen isotopic fractionations ($^{15}\varepsilon$)

The isotopic fractionation associated with photolysis for each experiment ($^{15}\varepsilon_n$, where n is the cut off wavelength or "Xe" for no filter) was determined from the Rayleigh plots generated using Eqs. (1) and (2). Most of the Rayleigh plots display a good correlation (typically with $R^2 > 0.8$). A typical example of a Rayleigh plot is shown in Figure 5. For experiments conducted for 7–12 days duration and with/without an UV filter, we derived $^{15}\varepsilon_{Xe}$, $^{15}\varepsilon_{280}$, $^{15}\varepsilon_{305}$, and $^{15}\varepsilon_{320}$ values of (−15 ± 1.2)‰, (−23.2 ± 1.0)‰, (−38.6 ± 2.8)‰, and (−47.9 ± 6.8)‰, respectively (Table III).

TABLE III. $^{15}\varepsilon$ values observed in this study and the values predicted by the ΔZPE-model of Frey *et al.*[9]

Filter type	Expt. $^{15}\varepsilon$ (±1σ)/‰	R^2	Model (ZPE-shift)$^{15}\varepsilon$/‰
Dark expt.	−4.2 ± 5.9	0.05	...
No filter (20.3 h)	−14.1 ± 1.0	0.95	...
No filter (162.8 h)	−16.0 ± 1.4	0.95	...
280 nm	−23.2 ± 1.0	0.98	−16.8
305 nm	−38.6 ± 2.8	0.95	−36.8
320 nm	−47.9 ± 6.8	0.83	−42.8

IV. DISCUSSIONS AND IMPLICATIONS

A. Isotopic fractionation

The isotopic fractionations obtained from all photolysis experiments are generally negative implying that the remaining nitrate in the snow is enriched in ^{15}N. However, the isotopic fractionations differ depending on the UV filter used in the experiment. For the two unfiltered Xe lamp experiments, the calculated average isotopic fractionation of $^{15}\varepsilon_{Xe} = (-15.0 \pm 1.2)‰$ is close to the result obtained by Blunier *et al.*[10] ($(-11.7 \pm 1.4)‰$). However, these laboratory results do not agree with the values observed in the field.[9,10,28] Our experimental studies show that the $^{15}\varepsilon_{Xe}$ value observed in the experimental study by Blunier *et al.*[10] is mainly due to significant excitation of the nitrate absorption band around 200 nm by the Xe lamp, in agreement with the explanation of Frey *et al.*[9] Surprisingly, the use of artificial snow and product recycling (due to a closed system) in the laboratory study from Blunier *et al.*[10] seem to have a minor impact on the isotopic fractionations. Since the mechanism of photolysis in the 200 nm band is most likely isomerization (with the possibility of decaying back to nitrate),[45] the isotope-dependent absorption cross section will be the major factor driving the fractionations. The use of UV filters was partly motivated by this observation and it has two important consequences. First, it avoids the excitation of the short wavelength absorption band where dissociation mechanisms are radically different from those occurring during the photoexcitation of the low energy band.[45] Second, it better replicates the solar UV at Dome C by shielding the 305 nm band.

According to solar irradiance measurements at Dome C on January 8, 2013 at 2 pm,[57] shown in Figure 2(a), the photolysis experiment conducted using the 320 nm filter is the best match to the field conditions of Dome C, in particular because it blocks the entire UV region below 300 nm. This experiment also gives the best agreement between laboratory experiments ($^{15}\varepsilon = (-47.9 \pm 6.8)‰$) and previous field studies conducted at Dome C for isotopic fractionations[9,10] and in the East part of the Antarctic Plateau ($^{15}\varepsilon$ range of -40.0 to $-74.3‰$[28]) (see Table IV).

TABLE IV. $^{15}\varepsilon$ values determined in different studies in comparison to observations made using an identical light spectrum (Xe and sun).

$^{15}\varepsilon$ ($\pm 1\sigma$)/‰	UV source	Reference
-15.0 ± 1.2	Xe lamp (no filter)	This study[a]
-11.7 ± 1.4	Xe lamp (no filter)	Blunier *et al.*[b]
-47.9 ± 6.8	Xe lamp (320 nm filter)	This study[a]
-40 to -74.3	Sun	Erbland *et al.*[c]

[a]Isotopic fractionation constant derived for the unfiltered Xe lamp experiment.
[b]Isotopic fractionation constant derived by Blunier *et al.*[10] for the unfiltered Xe lamp used in their experiment.
[c]Apparent isotopic fractionation constant observation range for the East Antarctic Plateau by Erbland *et al.*[34]
[d]Isotopic fractionation constant derived for the Xe lamp using the 320 nm filter in this laboratory study.

B. Theoretical approach

1. Comparison with the theoretical approach of Frey et al.

Frey[9] constructed a theoretical model to characterize the wavelength dependence of the observed fractionations. In this model, $^{15}\varepsilon_{pho}$ was estimated from the ratio of $^{15}NO_3^-$ and $^{14}NO_3^-$ photolysis rates; the absorption cross section of $^{15}NO_3^-$ was deduced using the cross section of $^{14}NO_3^-$ in water[43] using the Zero Point Energy shift (ΔZPE-shift) approach.[27,46] The model is based on the observation that, with substitution of a light isotope by a heavier one, the ground state vibrational zero point energy of the heavier $^{15}NO_3^-$ isotopologue is reduced. This difference in ZPE results in a blue shift of the UV absorption cross-section for the heavier isotopologue. Frey *et al.*[9] determined a ΔZPE of -44.8 cm^{-1} for $^{15}NO_3^-$ corresponding to an average blue shift of 0.5 nm of the absorption cross-section in the 280–360 nm spectral range. Using the experimental $^{14}NO_3^-$ cross-section of Chu *et al.*[43] the calculated cross-section of $^{15}NO_3^-$ (see above) and the solar actinic flux determined from the TUV model (TUV 4.4)[47] for Dome C conditions on January 15, 2004 at solar noon (03:45 UT),[58] Frey *et al.*[9] determined a photolytic $^{15}N/^{14}N$ isotopic fractionation of $-48‰$ which was close to the apparent isotopic fractionation observed in the field ($^{15}\varepsilon_{app} = (-60 \pm 15)‰$). These two values are of distinct nature. One is calculated from a single TUV-modeled spectrum and the other is an apparent value[9,28] accounting for processes arising from UV-photolysis (e.g., nitrate physical release from snow, deposition and removal by the wind) and for varying isotopic effects due to varying spectral distribution of the actinic flux throughout the sunlit season (varying solar zenith angle and thus UV-filtering through the atmosphere).

In this study, we first use the Frey *et al.*[9] model to predict the expected photolytic isotopic fractionations from our experiments performed with varying spectral distributions of the actinic flux irradiating the snow. For $\sigma(^{14}NO_3^-$, aqueous), we use the absorption cross section measured by Chu *et al.*[43] at 278 K. We use a variety of filters to provide specific spectral distributions which partially overlap the absorption cross sections of $^{14}NO_3^-$ and $^{15}NO_3^-$. The calculated fractionation constants are then compared to the corresponding experimental measurements in order to test the applied ZPE shift.

The nitrate absorption band centered at 200 nm is a factor of 1000 more intense than the 305 nm band (see Paper I).[32] Therefore, full interpretation of the experiments using the pure Xe lamp and the 280 nm long-pass filter, which allow significant photon fluxes at wavelengths shorter than 280 nm (Figure 2(b)), requires a model describing the cross sections of both transitions. Such a model is not developed in this paper for two reasons. First, the natural actinic flux in the polar region does not reach such short wavelengths and second, the solvation effect discussed below is likely very different for the bands centered at 200 nm and 305 nm. The first point is verified by considering the extreme case of the actinic flux received at an elevation of 4000 m, for a solar zenith angle of 35° (i.e., at its maximum for a latitude around 60° N or S) and

TABLE V. Comparison of the experimental $^{15}N/^{14}N$ fractionations with the modeled values (the approach of Frey *et al.*[9]) but with two different ΔZPE values for the 305 nm and 320 nm filters.

Filter type (nm)	$(^{15}\varepsilon_{exp}\pm1\sigma)$/‰	$^{15}\varepsilon_{mod}$/‰, Frey *et al.*, ΔZPE = −44.8 cm^{-1}	$^{15}\varepsilon_{mod}$/‰, Frey *et al.*, ΔZPE = −51 cm^{-1}
305	−38.6 ± 2.6	−34.6	−39.3
320	−47.9 ± 6.8	−41.2	−46.8

for an ozone column of 85 DU (i.e., slightly lower than the lowest column observed at South Pole in October 1993, 89 DU). To verify this, we used version 4.2 of the TUV model with a surface albedo of 0.9 (spectrum not shown).

Table V shows the comparison of the calculated photolytic $^{15}N/^{14}N$ isotopic fractionations and the corresponding laboratory observation for the 305 nm and the 320 nm filters. We observe that a ΔZPE-shift of −44.8 cm^{-1} underestimates the absolute value of the observed isotopic fractionations. To reconcile the experimental observations with this simple model, a ΔZPE-shift value of −51 cm^{-1} must be used, which is clearly too large when compared to our best estimate of (−47.5 ± 1.0) cm^{-1} (see Appendix B).

We conclude that the ΔZPE-shift model combined with the above mentioned actinic flux cannot explain the nitrogen isotopic fractionations observed at Dome C or in the present lab experiments using the 305 nm and 320 nm filters. For these reasons, an improved description of the absorption cross section of $^{15}NO_3^-$ derived from the one of $^{14}NO_3^-$ is presented below.

2. Additional constraints for the absorption cross-sections for $^{14}NO_3^-$ and $^{15}NO_3^-$

A more accurate description of the effect of isotopic substitution on the amplitude and shape of the NO_3^- absorption cross section at 303 nm was obtained using a four parameter analytical model.[31] The model is introduced here and detailed in Appendix B. The model calculates $\sigma(E)/E$, the low resolution absorption cross-section $\sigma(E)$ divided by the photon energy E, and represents it using a modified Gaussian function that depends on four parameters, A, C, W, and S. The analytical model was used to fit the 5 cross sections of aqueous $^{14}NO_3^-$ measured by Chu *et al.*[43] at different temperatures, for wavelengths above 285 nm ($E < 35\,000$ cm^{-1}). For each temperature, the set of 4 parameters are given in Table VI.

TABLE VI. Four parameters derived from the analytical model (using Eq. (B1)) applied to the 5 cross sections of aqueous $^{14}NO_3^-$ measured in Chu *et al.*[43] at different temperatures. The asymmetry parameter is set to 0.9.

	Parameters of $\sigma(E)/E$		
T/K	A/(10^{-25} cm^2 cm^{-1})	C/cm^{-1}	W/cm^{-1}
278	7.360	34 052.0	3573.0
283	7.318	34 035.5	3575.0
288	7.284	34 019.7	3578.9
293	7.215	34 007.2	3581.1
298	7.192	34 001.1	3592.0

The analytical cross section of aqueous $^{15}NO_3^-$ at the same temperature is obtained based on the $^{14}NO_3^-$ cross section using a series of physical arguments detailed in Appendix B: uniformly increase the amplitude by 1.0%, shift the center towards high energies by 32.5 cm^{-1} and reduce the width via an energy scale factor of 1.0%, starting from the new center. The factor 1.0% is varied in the [0.9, 1.1]% range to account for the uncertainty in the determination of this parameter. The ΔC shift parameter is varied in the range [−28.5, −36.5] cm^{-1} to account for uncertainties among which the $\Delta ZPE_{excited}$ is dominant (cf. Appendix B). As in Sec. IV B 1, we only consider the laboratory experiments using the 305 and 320 nm filters, for which only the 305 nm absorption band contributes to the photolysis.

Table VII shows that the ΔC value of −32.5 cm^{-1} and a width reduction factor of 1.0% lead to a good match with the observation experimental $^{15}\varepsilon$ values for both the 305 nm and 320 nm filters. ΔC drives most of the isotope fractionation, an effect which is about twice that of the width reduction of 1.0%. ΔC and the width reduction effects appear to be almost cumulative when comparing the three cases where only the ΔC contribution, only the width reduction contribution, or both contributions together.

3. Solvation and temperature effects: NO_3^- dissolved in water at 5 °C (278 K) versus NO_3^- in snow at −30 °C

The model approach conducted above uses the cross section of aqueous nitrate at 278 K (5 °C). Therefore, the cross section derived for the least abundant isotopologue is $\sigma(^{15}NO_3^-$, aq., +5 °C). To extend this result to nitrate in snow at −30 °C, it is necessary to investigate the differential effects on the cross sections of $^{15}NO_3^-$ and $^{14}NO_3^-$ due to the change in temperature from +5 °C to −30 °C, as well

TABLE VII. Modelled $^{15}N/^{14}N$ fractionations obtained when ΔC and the width reduction factor are varied (305 nm and 320 nm filters at the top and bottom of each cell, respectively). The experimentally observed $^{15}\varepsilon$ values are given as a comparison.

		$^{15}\varepsilon_{mod}$/‰ for T = 278 K		
Filter type (nm)	$(^{15}\varepsilon_{exp}\pm1\sigma)$/‰	$\Delta C = 0$ cm^{-1}, W reduction = (1.0 ± 0.1)%	$\Delta C = (-32.5 \pm 4)$ cm^{-1}, W reduction = 0%	$\Delta C = (-32.5 \pm 4)$ cm^{-1}, W reduction = 1.0%
305	−38.6 ± 2.6	−12.3 ± 1.4	−23.9 ± 3.1	−38.0 ± 3.2
320	−47.9 ± 6.8	−17.4 ± 2.0	−28.0 ± 3.8	−47.8 ± 3.7

TABLE VIII. The dependence of the modeled nitrogen isotopic fractionations on water temperature and comparison with values obtained for the 305 nm and the 320 nm filter experiments.

		$^{15}\varepsilon_{mod}$/‰, $\Delta C = -32.5$ cm^{-1}, 1.0% factor				
Filter type (nm)	($^{15}\varepsilon_{exp}\pm1\sigma$)/‰	278 K	283 K	288 K	293 K	298 K
305	-38.6 ± 2.6	−38.0	−37.7	−37.3	−37.1	−36.8
320	-47.9 ± 6.8	−47.8	−47.4	−47.0	−46.7	−46.4

as the difference between the solvation effects of nitrate deposed in/on snow with those in water solution. The solvation effect is assumed here to be very similar for both $^{14}NO_3^-$ and $^{15}NO_3^-$. Ideally, the absorption cross section of the (unsolvated) gas phase NO_3^- anion should be taken as a reference to characterize various degrees of water solvation expected in snow but this gas phase NO_3^- cross section has never been measured.

To account for the temperature effect, we compare the fractionations obtained with modeled cross sections of $^{14}NO_3^-$ and $^{15}NO_3^-$, at five temperatures from 278 K to 298 K. Table VIII shows that the temperature dependence of the modeled nitrogen fractionation constants is weak and linear with a sensitivity of 0.06 ‰/K and 0.07 ‰/K for the 305 nm and 320 nm filters, respectively. Considering "aqueous nitrate" at −30 °C, we anticipate that the modeled $^{15}\varepsilon$ values will be 2.1 and 2.4‰ lower than the values at 5 °C for the two filters. This effect is small with respect to both our experimental and modeled cross section uncertainties.

The role of nitrate solvation is analyzed in terms of dependence of the $^{14}NO_3^-$ absorption cross sections on the degree of solvation. The absorption cross section of NO_3^- is only well known for bulk water. Considering nitrate in snow, this species can reside in various microphysical locations such as at the air/snow grain interface, in a disordered interface or within the grain. The different microscopic environments of nitrate can impact its photolability (see Paper I[32]) but they will also impact its solvation interactions. The solvent shift of absorption cross section of NO_3^- deposited at the water/air or at the ice/air interfaces is not well known and it is more complicated for the case where NO_3^- resides in/on a snow grain. If we assume that each grain of ice is surrounded by a thin layer of water,[48] we may approximate that the solvation shift is half that of bulk water. Moreover, studies of the solvation effect on the NO_3^- absorption cross sections consider the strong $\pi^* \leftarrow \pi$ electronic transition[49] located around 200 nm and not the much weaker $\pi^* \leftarrow$ n transition located around 305 nm.[50,51] To investigate the potential effect of the solvation shift on the modeled nitrogen isotope fractionation, we consider solvation shifts of −100 and +100 cm^{-1} (for both $^{14}NO_3^-$ and $^{15}NO_3^-$) and compare the modeled $^{15}\varepsilon$ values to the simple case where there is no solvation shift. We keep the other parameters as in the above paragraph, i.e., using $\Delta C = -32.5$ cm^{-1}, the 1.0% width reduction factor as well as $\sigma(^{14}NO_3^-$, aq. T = 278 K). Table IX shows that the dependence on the solvation effect is small if the solvation shift in snow is limited to ±100 cm^{-1} (i.e., approx. ±0.9 nm) from the one of bulk water: the modeled changes are ±1.9 and ±2.2‰ for the 305 and 320 nm filters respectively. The changes in $^{15}\varepsilon_{mod}$ are smaller than the uncertainty in the experimental $^{15}\varepsilon$ values and of the same order of magnitude as the changes resulting from the uncertainty in ΔC (Table VII). The weak sensitivity of $^{15}\varepsilon$ to solvation shifts (i.e., due to the different phase of nitrate but also potentially due to different nitrate locations in snow) simplifies the interpretation of nitrate nitrogen isotope profiles in Antarctic snow since we can assume to first order that nitrate solvation (e.g., due to different nitrate microscopic chemical domains as discussed in Paper I[32]) has no significant impact of the global N isotope fractionation.

Figure 6 shows the modeled spectral nitrogen isotope fractionation ($^{15}\varepsilon(\lambda)$) for $\Delta C = -32.5$ cm^{-1} and a 1.0% width reduction factor, as well as for the extreme cases when ΔC and the width reduction factor are varied to the extremity of their segments. Overall, we observe that the changes in $^{15}\varepsilon(\lambda)$ are moderate. Using the $^{14}NO_3^-$ and $^{15}NO_3^-$ absorption cross sections computed in this study as well as the TUV modeled actinic flux from Frey *et al.*[9] for January 15, 2004, we determine a photolytic isotopic fractionation of −55.1‰ which was close to the apparent fractionation constant observed in the field ($^{15}\varepsilon_{app} = (-60 \pm 15)$‰).

A comparison of the recommended spectral nitrogen isotope fractionation ($^{15}\varepsilon(\lambda)$) derived in this study and the distribution obtained from the experimental measurement of the absorption cross sections of aqueous $^{15}NO_3^-$ and $^{14}NO_3^-$ is shown in Figure 6. The variations of both the modeled and experimental curves agree with positive $^{15}\varepsilon$ values below 308 nm.

TABLE IX. Impact of the solvation shift on the modeled nitrogen isotope fractionation for the 305 nm and the 320 nm filters.

		$^{15}\varepsilon_{mod}$/‰, $\Delta C = -32.5$ cm^{-1}, 1.0% factor, T = 278 K, various solvation shifts		
Filter type (nm)	($^{15}\varepsilon_{exp}\pm1\sigma$)/‰	−100 cm^{-1}	0 cm^{-1}	+100 cm^{-1}
305	-38.6 ± 2.6	−36.2	−38.0	−39.9
320	-47.9 ± 6.8	−45.7	−47.8	−50.0

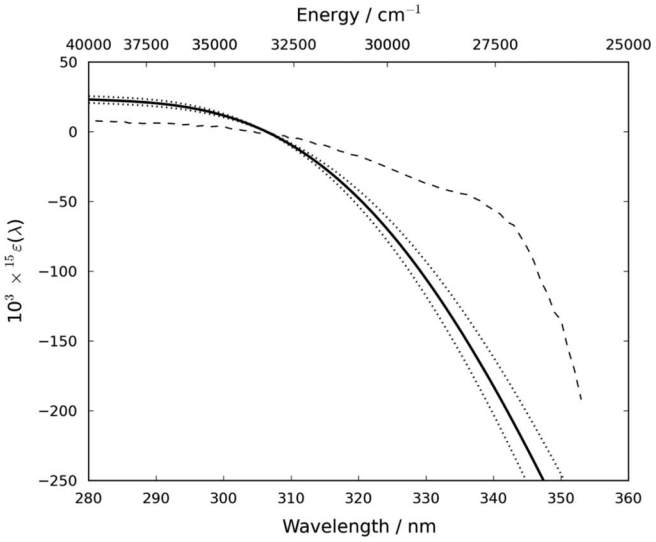

FIG. 6. Spectral nitrogen isotope fractionation ($^{15}\varepsilon(\lambda)$) determined from the ratio of the recommended absorption cross sections of $^{14}NO_3^-$ and $^{15}NO_3^-$ in snow ($\Delta C = -32.5$ cm^{-1} and 1.0% width reduction). The dotted lines represent the extreme cases ($\Delta C = -28.5$ cm^{-1}/1.0% and $\Delta C = -36.5$ cm^{-1}/1.1%). An experimental determination of $^{15}\varepsilon(\lambda)$ from aqueous nitrate is shown for comparison (dashed line. Caveats in this measurement are discussed in the text).

Finally, we recall that the 280 nm filter was not used to constrain our model. In order to test our computed $^{15}NO_3^-$ cross section, filters cutting at wavelengths above 280 nm (and above 320 nm) can be used in future studies. However, in order to obtain sufficient nitrate loss, very long experiments (with durations of several weeks) would have to be conducted.

V. SUMMARY AND CONCLUSION

Photolytic fractionation of nitrate isotopologues in natural snow was studied in a series of experiments. Analysis of the nitrogen isotope ratios in nitrate as a function of depth in the snow column resulted in $^{15}\varepsilon_{Xe}$, $^{15}\varepsilon_{280}$, $^{15}\varepsilon_{305}$, and $^{15}\varepsilon_{320}$ values of (-15 ± 1.2)‰, (-23.2 ± 1.0)‰, (-38.6 ± 2.8)‰, and (-47.9 ± 6.8)‰ for unfiltered Xe lamp and 280, 305, and 320 nm filters, respectively. The isotopic fractionation constant determined for the unfiltered Xe lamp is in good agreement with the previously determined value of (-11.7 ± 1.4)‰ by Blunier *et al.*[10] This result is attributed to excitation of the strong transition of nitrate around 200 nm, this excitation is strongly attenuated in nature by atmospheric O_2 and O_3. The observed *in situ* photolysis is thus only due to the photoexcitation around 305 nm and results in significant nitrogen isotopic fractionation that is strongly dependent on the wavelength spectrum of irradiation, with more negative values as the actinic flux spectrum is red shifted, in agreement with the prediction by Frey *et al.*[9] Our study has shown that isotopic exchange and chemical reaction between NO_x photoproducts and the snow nitrate is insignificant. A model of the depth resolved photolytic isotopic fractionation shows $^{15}\varepsilon_{photo}$ is insensitive to depth in the snow column, even when a significant decrease in the actinic flux is observed with depth. This is in agreement with the near wavelength independent e-folding depths reported by Paper I.[32] We have also presented a new model for determining the absorption cross-section of $^{15}NO_3^-$ from $^{14}NO_3^-$ that improves the ZPE-shift model[9] and described the parameters to be considered to interpret nitrogen isotopic fractionations. First, changes in shape (width and amplitude) of the absorption cross-section due to ^{14}N to ^{15}N isotope substitution must be taken into account through a 1.0% width reduction factor and 1.0% amplitude increase. Second, the center shift of the cross section center is expected to be in the range $[-28.5, -36.5]$ cm^{-1}; the large uncertainty in this parameter mainly arises from insufficient knowledge of $\Delta ZPE_{excited}$. The ΔZPE of NO_3^- in its excited electronic state has been ignored up to now. The solvation and temperature effects on the absorption cross-section of nitrate are probably weak relative to uncertainties in the parameters used to derive the cross section of $^{15}NO_3^-$ (ΔC and width reduction factor). Therefore, for the analysis of N isotope fractionation associated with nitrate photolysis in snow in polar regions (actinic fluxes cut above 280 nm), we recommend the absorption cross section of nitrate in liquid water at 278 K (Chu *et al.*[43]) for $\sigma(^{14}NO_3^-$, in snow) and to model the ^{14}N to ^{15}N isotope substitution by using a global $\Delta C = -32.5$ cm^{-1} and a 1.0% width reduction factor. The $\Delta C = -32.5$ cm^{-1} value may be seen as an apparent shift in the center since it integrates the poorly known but weak temperature and solvation effects described above.

ACKNOWLEDGMENTS

The research leading to these results has received funding from the European Community's Seventh Framework Programme (FP7/2007–2013) under Grant Agreement No. 237890 (J.S., T.A.B., C.M., M.S.J.). We would like to thank INSU through its LEFE program for its financial support for lab experiments (J.S., T.A.B.). The Agence nationale de la recherche (ANR) is gratefully acknowledged for its financial support through the OPALE project (Contract No. NT09–451281) (J.S., T.A.B.). This work has been also supported by a grant from Labex OSUG@2020 (Investissements d'avenir – ANR10 LABX56) (J.S., T.A.B.). Access to the Dome C site was possible with the financial support of the Institut Polaire Française Paul Emile Victor (IPEV) through the program 1011 (SUNITEDC) (J.S., T.A.B.). We would like to thank Ghislan Picard and Quentin Libois for providing irradiance measurements at Dome C, Antarctica. Our gratitude also goes to Susanne Preunkert, Nicolas Caillon, Samo Tamse, Patrick Ginot, Dimitri Osmont, and Florent Dominé for their significant contribution and help in this study.

APPENDIX A: THE NITRATE MASS AND STABLE ISOTOPE RATIOS MEASURED AT THE END OF THE DIFFERENT EXPERIMENTS

Figures 7 and 8 show the nitrate mass fraction left in the snow and the $\delta^{15}N$ values at the end of the control experiments. Figures 9–11 show the variation in the actual concentration of nitrate as well as the $\delta^{18}O$ and $\Delta^{17}O$ at the end of each photolysis experiment with the different filters.

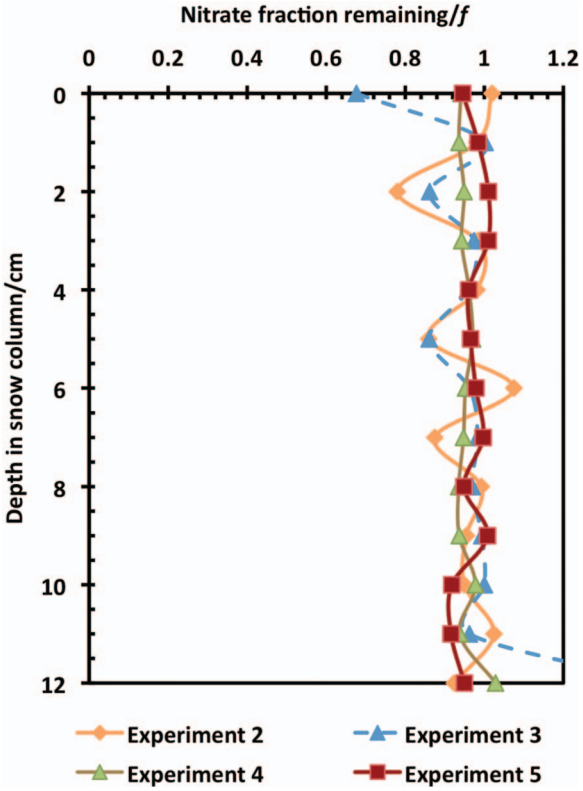

FIG. 7. The nitrate concentration profile for control experiments with depth for Experiment 2 (case 2: Temperature cycle), Experiment 3 (case 3: NO_2 ^{15}N-exchange in dark), Experiment 4 (case 4: NO_2 reactivity in UV-light/air-zero), and Experiment 5 (case 5: NO ^{15}N-exchange in dark).

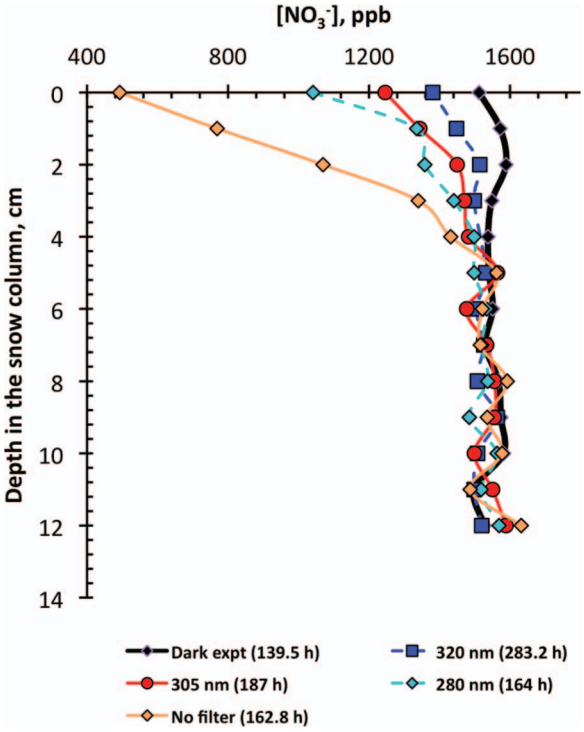

FIG. 9. Plot of nitrate concentration for each experiment versus depth in the snow column.

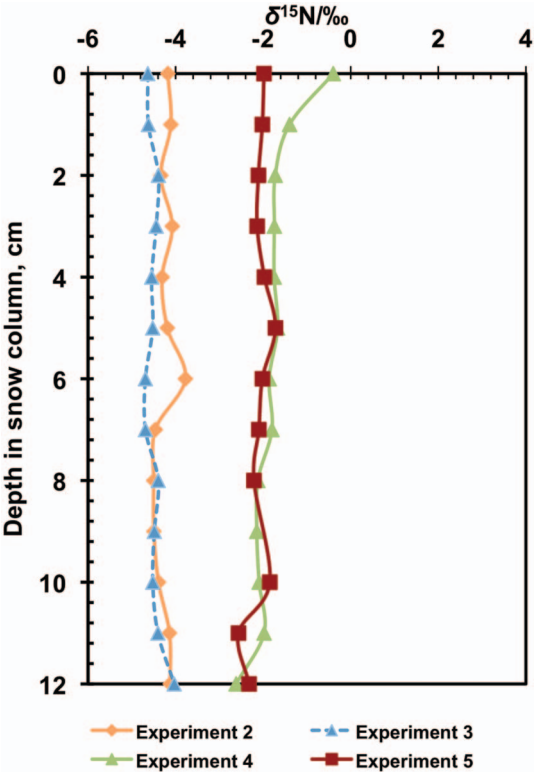

FIG. 8. The $\delta^{15}N$ profile for control experiments with depth for Experiment 2 (case 2: Temperature cycle), Experiment 3 (case 3: NO_2 ^{15}N-exchange in dark), Experiment 4 (case 4: NO_2 reactivity in UV-light/air-zero), and Experiment 5 (case 5: NO ^{15}N-exchange in dark).

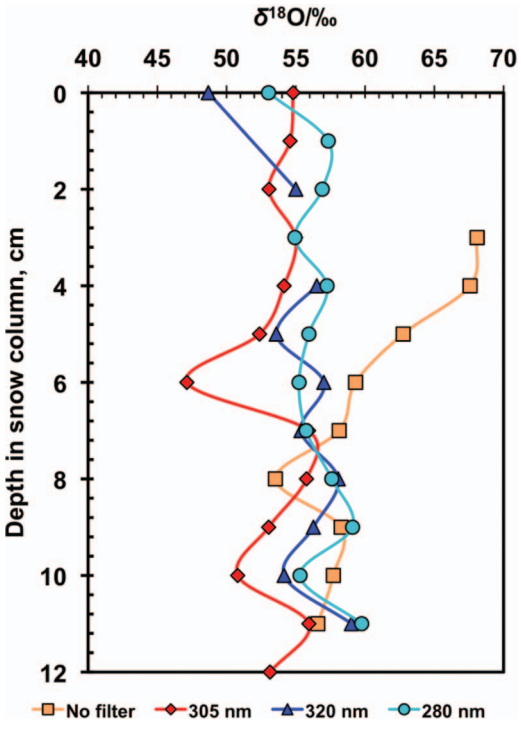

FIG. 10. Plot of $\delta^{18}O$ versus depth in the snow column.

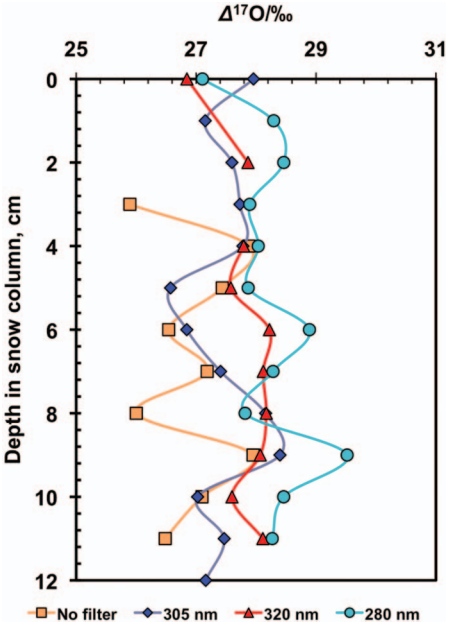

FIG. 11. Plot of the $\Delta^{17}O$ values versus depth in the snow column.

APPENDIX B: DERIVATION OF THE $^{15}NO_3^-$ CROSS SECTION FROM THE $^{14}NO_3^-$ CROSS SECTION

The ΔZPE-shift model[9] is approximate and a more accurate description of the effect of isotopic substitution on the absorption cross section of a molecular electronic transition has been made. A four-parameter analytic model[31] derived from the reflection principle[53] has been used to obtain the $^{15}NO_3^-$ cross section from that measured for $^{14}NO_3^-$. This approach has been previously used to compare the cross sections of the Hartley band of 18 isotopologues of ozone.[30] In this model, $\sigma(E)/E$, the low resolution absorption cross-section $\sigma(E)$ divided by the photon energy E, is approximated by a modified, asymmetric Gaussian function[31] depending on four parameters, A, C, W, and S:

$$\sigma(E)/E = A(1 - SX)\exp[-X^2(1 - SX + 0.5(SX)^2)], \quad \text{(B1)}$$

where $X = (E\text{-}C)/W$ and S are dimensionless quantities.

The amplitude A depends mostly on the transition dipole moment which is unknown, but we can use the experimental cross section to determine A. The center C is the vertical excitation energy minus the ZPE corrections detailed below; the ZPE corrections vary from one isotopologues to the other. The width W depends on the six ratios of the six widths of the ground state wave function divided by the corresponding slopes of the upper Potential Energy Surface (PES) (here a 6D PES for NO_3^-) at the ground state equilibrium geometry. The asymmetry S depends on the curvatures (or the Hessian components) of the upper PES.[31,53] The dependence of the four parameters (A, C, W, and S) on isotopic substitution can be estimated from spectroscopic data such as the ZPE or the vibrational frequencies and/or from analogy with the parameters of other molecules. Note that the ΔZPE-shift model used above corresponds to the simple case where only the center C is modified and then the A, W, and S parameters are assumed to be constant under isotope substitution.

In order to derive the $^{15}NO_3^-$ absorption cross section we have fitted the four parameters of the analytic model to the experimental $^{14}NO_3^-$ cross sections of Chu *et al.*[43] measured at 278 K, 283 K, 288 K, 293 K, and 298 K. Due to the overlap between the two electronic bands centered at 305 nm and 200 nm, we have only fitted the range from 285 nm to 360 nm where the contribution from the 200 nm band is negligible. The sets of four fitted parameters corresponding to the four cross sections from 278 K to 293 K vary smoothly, allowing extrapolation down to 243 K, from which the cross section of $^{14}NO_3^-$ (243 K) has been calculated using Eq. (B1).

A corresponding set of four parameters will determine the cross section of $^{15}NO_3^-$ at 243 K. The approach is to predict the isotopologue shift of these four parameters using: (a) information derived from the reflection principle, (b) experimental vibrational frequencies, and (c) information derived from absorption cross sections of a set isotopologues of ozone.

The absorption band center parameter, C_{abc}, which defines the center of $\sigma_{abc}(E)/E$ where σ is the absorption cross section of a given electronic transition, E is the photon energy (usually in cm^{-1}), and abc designs a specific isotopologues, is given by

$$C_{abc} = T_e - \Delta C_{abc}, \quad \text{(B2)}$$

where T_e, the vertical excitation energy, is a constant independent of the considered isotopologue and ΔC_{abc}, the shift of C specific to *abc*, is given by

$$\Delta C_{abc} = \Delta ZPE_{\text{ground-abc}} - \Delta ZPE_{\text{excited-abc}}, \quad \text{(B3)}$$

where "ground" and "excited" mean the ground and excited electronic states.

A dominant isotopologue is taken the reference (noted ref.) and shift (s) are determined for the other abc isotopologue (s):

$$\Delta ZPE_{\text{ground-abc}} = ZPE_{\text{ground-ref}} - ZPE_{\text{ground-abc}}, \quad \text{(B4)}$$

$$\Delta ZPE_{\text{excited-abc}} = ZPE_{\text{excited-ref}} - ZPE_{\text{excited-abc}}. \quad \text{(B5)}$$

The ZPE_{ground} are usually approximated either by half the sum of the experimental vibrational frequencies (in which case ZPE_{ground} is underestimated) or by the half sum of the harmonic frequencies (in which case ZPE_{ground} is overestimated) because the anharmonic corrections are unknown and therefore neglected in both cases.

By analogy with diatomic molecules, $ZPE_{excited}$ has been omitted until now as the excited PES of polyatomic molecules is dissociative. In fact, the excited PES has 3N-6 dimensions, among which some coordinate(s), are bound at (or near) the equilibrium geometry of the ground state. The Hartley band of ozone is used below as an example. The Hartley absorption cross sections of 18 ozone isotopologues were obtained numerically using the Multi Channel Time Dependent Hartree (MCTDH) method.[30] For each of these isotopologues, we have determined by a fit the sets of four parameters, A, C, W, and S, of the analytic model of Eq. (B1). The values of A, C, W, S, and ZPE are given in Table II of Ref. 32.

The dependencies of these four parameters on the oxygen isotopic composition have been analyzed. The effect of

central oxygen substitution on the *A*, *C*, and *W* parameters is about 1.7 to 1.8 times larger than the effect of a terminal substitution. A similar (and larger) effect is expected for a ^{14}N to ^{15}N substitution in NO_3^- because the central N atom is involved in three bonds and therefore has a larger relative effect on the vibrational frequencies and on therefore on the ZPE. For example, consider the ^{16}O to ^{17}O central oxygen substitution, from $^{16}O_3$ to $^{16}O^{17}O^{16}O$, for which the four parameters, *A*, *C*, *W,* and *S*, vary as follows: (a) the amplitude, *A*, increases by the factor of +0.8%; (b) the width parameter, *W*, decreases by the opposite factor of −0.8%; (c) the center *C* is blue shifted to higher energy by $\Delta C = 15.3\ cm^{-1}$ (this value, equal to 0.78 times the ΔZPE_{ground} of 19.7 cm^{-1}, is discussed below); (d) the asymmetry parameter *S* decreases by about 0.5%. The opposite variations of *A* and *W* occurs because the area of $\sigma(E)/E$, which is proportional to the product of *A* and *W*, should be conserved when the transition dipole moment is constant (this approximation is almost valid case for the Hartley band).

The 0.78 reduction in ΔC, compared with ΔZPE_{ground} which is expected with the ΔZPE-shift model, is attributed to the contribution of $\Delta ZPE_{excited}$ (see Eq. (B3)) which is usually neglected when the upper PES is only dissociative.[53] This $\Delta ZPE_{excited}$ should be taken into account because the upper PES of the Hartley band of ozone is only dissociative along the two O–O coordinates, but is bound along the O–O–O angular coordinate[54] with a force constant similar to that of the ground state, and with a bending frequency similar to that in the ground state. Consequently, ZPE_{ground} ($^{16}O_3$) $= \frac{1}{2}(\nu_1+\nu_2+\nu_3)$ and $ZPE_{excited}(^{16}O_3) \approx \frac{1}{2}(\nu_{2ex})$ and ZPE_{ground} ($^{16}O^{17}O^{16}O$) $= \frac{1}{2}(\nu'_1 + \nu'_2 + \nu'_3)$ and $ZPE_{excited}(^{16}O^{17}O^{16}O) \approx \frac{1}{2}(\nu'_{2ex})$ where the prime refers to the $^{16}O^{17}O^{16}O$ substituted species. The ΔZPE_{ground} between $^{16}O_3$ and $^{16}O^{17}O^{16}O$ is 19.7 cm^{-1} and the corresponding value of ΔC is 15.3 cm^{-1}, leading to $\Delta ZPE_{excited} = \Delta ZPE_{ground} - \Delta C = 19.7 - 15.3 = 4.4\ cm^{-1}$.

The shifts of the *A*, *C*, *W*, *S* parameters due to the ^{16}O to ^{17}O substitution in ozone have been transposed to the case of the ^{14}N to ^{15}N substitution for NO_3^- using some assumptions and approximations described below. We used the six observed vibrational frequencies[9] of $^{14}NO_3^-$ and $^{15}NO_3^-$ to estimate both the corresponding ΔZPE_{ground} and $\Delta ZPE_{excited}$. The $\Delta ZPE_{ground} = 44.8\ cm^{-1}$ used by Frey *et al.*[9] is derived from these experimental vibrational frequencies without correction of the 21 x_{ij} vibrational anharmonicities. An estimate of this anharmonic contribution from the six x_{ij} of NO_2[55] and/or those of O_3[56] gives a correction of $+2.7 \pm 1\ cm^{-1}$, leading to a new value of $\Delta ZPE_{ground} = 47.5 \pm 1\ cm^{-1}$. The determination of $\Delta ZPE_{excited}$ is much more difficult because we do not have the 6D PES of the excited state. For the ground state equilibrium geometry, the 6D excited PES is expected to be dissociative along the three equivalent N–O stretch coordinates and bound along the three angles. Consequently, there is no contribution from the three stretching coordinates to $ZPE_{excited}$ and the three (non-dissociative) angular coordinates are associated with the three unknown bending frequencies of the excited PES. We have assumed that the sum of these three frequencies is at most equal to those of the ground state.

Therefore, using the six vibrational frequencies of $^{14}NO_3^-$ and those of $^{15}NO_3^-$, $\Delta ZPE_{excited}$ is at most 17.5 cm^{-1} corresponding to 37% of the ΔZPE_{ground}, and $\Delta ZPE_{excited}$ is therefore expected to be $15 \pm 3\ cm^{-1}$ because the bond strengths in the excited state are lower than those of the ground state. The resulting ΔC is then $\Delta C = 47.5 - 15 = (32.5 \pm 4)\ cm^{-1}$. Note that $\Delta ZPE_{ground} = 44.8\ cm^{-1}$ between $^{14}NO_3^-$ and $^{15}NO_3^-$ is about two times larger than the value of 19.7 cm^{-1} between $^{16}O_3$ to $^{16}O^{17}O^{16}O$, mainly because NO_3^- has six modes of vibration instead of three for O_3.

The vibrational frequencies of NO_3^-, O_3, and NO_2 are rather similar implying that the force constants are also similar. Moreover, the bending frequencies are always smaller than the stretch frequencies by a factor of 0.6–0.8 for these three molecules. These observations justify the use of results obtained for O_3 and NO_2 for the NO_3^- molecule even if the number of vibrational degrees of freedom is two times larger for NO_3^-.

The shifts between the *A*, *W*, and *S* parameters of $^{14}NO_3^-$ and $^{15}NO_3^-$ have been obtained from those derived for the $^{16}O_3$ to $^{16}O^{17}O^{16}O$ substitution discussed above: (a) the width has been reduced by 1.0% as explained below; (b) the amplitude has been increased by 1.0% to maintain the same area of $\sigma(E)/E$ for the two isotopologues; (c) the center has been shifted (a blue shift) by $\Delta C = 32.5\ (\pm 4)\ cm^{-1}$, as explained above; (d) the asymmetry parameter has been reduced by about 0.5%, from 0.9 to 0.895, deduced from the ozone results. This shift of 0.005 for *S* has a minor impact compared with the shifts of *C* and *W*, and its uncertainty will not be discussed. The 1.0% reduction of the width parameter from $^{14}NO_3^-$ to $^{15}NO_3^-$ (instead of 0.8% in the case of $^{16}O_3$ to $^{16}O^{17}O^{16}O$ ozone substitution) arises from three factors: (a) the variation of the mass is 13% higher for the ^{14}N to ^{15}N substitution than for ^{16}O to ^{17}O substitution; (b) the relative variation of mass from $^{14}NO_3^-$ to $^{15}NO_3^-$ is smaller by 20% compared to that from $^{16}O_3$ to $^{16}O^{17}O^{16}O$; (c) the nitrogen atom is more "central" because it has three chemical bonds of instead of two for the central oxygen atom of ozone. The "number of bonds" scaling factor has been checked in ozone by comparing the effect of a central substitution (from $^{16}O_3$ to $^{16}O^{17}O^{16}O$) with a terminal substitution (from $^{16}O_3$ to $^{17}O^{16}O^{16}O$) in which the width is reduced only by 0.44% instead of 0.8% as for the central substitution. A crude scaling of these two factors gives a reduction of 1.07% for the case of three bonds. This reduction factor should be corrected by +13% and −20% to take into account the mass effects described above in (a) and (b), leading to the global width reduction factor of 1% from $^{14}NO_3^-$ to $^{15}NO_3^-$ given above.

The modeled cross sections of $^{14}NO_3^-$ and $^{15}NO_3^-$ have been derived from the analytic model of Eq. (B1) using the two set of four parameters which are given in Table X, as a function of energy and wavelength to calculate the corresponding excitation rates due to the actinic flux and the related enrichments. The central information for the isotopologues enrichments is the ratio of the $^{14}NO_3^-$ and $^{15}NO_3^-$ cross sections which is shown in Figure 6. This ratio is smooth only because it is the ratio of two smooth analytic functions obtained with Eq. (B1). The ratio of the true cross

TABLE X. Model parameters defining the absorption cross sections of $^{14}NO_3^-$ and $^{15}NO_3^-$ at 243 K.

	Parameters of $\sigma(E)/E$ at 243 K			
Isotopologue	$A/(10^{-25}$ cm^2/cm$^{-1})$	C/cm^{-1}	W/cm^{-1}	S
$^{14}NO_3^-$	7.360	34 052.0	3573.0	0.9
$^{15}NO_3^-$	7.433	34 084.5	3537.3	0.895

sections may have oscillations due to isotopologue-dependent vibronic structure. The resulting oscillations of the cross section ratio are only important when a narrow excitation source is used. The actinic flux is a broad spectral source which is expected to average the possible oscillations of the cross section ratio due to vibronic structures.

[1] G. Michalski, Z. Scott, M. Kabiling, and M. H. Thiemens, Geophys. Res. Lett. **30**, 1870, doi:10.1029/2003GL017015 (2003).
[2] J. Savarino, J. Kaiser, S. Morin, D. M. Sigman, and M. H. Thiemens, Atmos. Chem. Phys. **7**, 1925 (2007).
[3] M. Legrand, E. Wolff, and D. Wagenbach, Ann. Glaciol. **29**, 66 (1999).
[4] E. W. Wolff, *Nitrate in Polar Ice*, Ice Core Studies of Global Biogeochemical Cycles (Springer-Verlag, Berlin, 1995).
[5] T. H. E. Heaton, Tellus B **42**, 304 (1990).
[6] M. G. Hastings, E. J. Steig, and D. M. Sigman, J. Geophys. Res., [Atmos.] **109**, D20306, doi:10.1029/2004JD004991 (2004).
[7] J. E. Dibb and S. I. Whitlow, Geophys. Res. Lett. **23**, 1115, doi:10.1029/96GL01039 (1996).
[8] R. Röthlisberger, M. A. Hutterli, S. Sommer, E. W. Wolff, and R. Mulvaney, J. Geophys. Res., [Atmos.] **105**, 20565, doi:10.1029/2000JD900264 (2000).
[9] M. M. Frey, J. Savarino, S. Morin, J. Erbland, and J. M. F. Martins, Atmos. Chem. Phys. **9**, 8681 (2009).
[10] T. Blunier, G. L. Floch, H. W. Jacobi, and E. Quansah, Geophys. Res. Lett. **32**, L13501, doi:10.1029/2005GL023011 (2005).
[11] R. Röthlisberger, M. A. Hutterli, E. W. Wolff, R. Mulvaney, H. Fischer, M. Bigler, K. Goto-Azuma, M. E. Hansson, U. Ruth, M. L. Siggaard-Andersen, and J. P. Steffensen, Ann. Glaciol.-Ser. **35**, 209 (2002).
[12] E. W. Wolff, A. E. Jones, T. J. Martin, and T. C. Grenfell, Geophys. Res. Lett. **29**, 1944, doi:10.1029/2002GL015823 (2002).
[13] A. E. Jones, R. Weller, P. S. Anderson, H. W. Jacobi, E. W. Wolff, O. Schrems, and H. Miller, Geophys. Res. Lett. **28**, 1499, doi:10.1029/2000GL011956 (2001).
[14] R. E. Honrath, M. C. Peterson, S. Guo, J. E. Dibb, P. B. Shepson, and B. Campbell, Geophys. Res. Lett. **26**, 695, doi:10.1029/1999GL900077 (1999).
[15] Y. H. Wang, Y. Choi, T. Zeng, D. Davis, M. Buhr, L. G. Huey, and W. Neff, Atmos. Environ. **41**, 3944 (2007).
[16] A. M. Grannas, A. E. Jones, J. Dibb, M. Ammann, C. Anastasio, H. J. Beine, M. Bergin, J. Bottenheim, C. S. Boxe, G. Carver, G. Chen, J. H. Crawford, F. Domine, M. M. Frey, M. I. Guzman, D. E. Heard, D. Helmig, M. R. Hoffmann, R. E. Honrath, L. G. Huey, M. Hutterli, H. W. Jacobi, P. Klan, B. Lefer, J. McConnell, J. Plane, R. Sander, J. Savarino, P. B. Shepson, W. R. Simpson, J. R. Sodeau, R. von Glasow, R. Weller, E. W. Wolff, and T. Zhu, Atmos. Chem. Phys. **7**, 4329 (2007).
[17] H. W. Jacobi and B. Hilker, J. Photoch. Photobiol., A **185**, 371 (2007).
[18] H. W. Jacobi, T. Annor, and E. Quansah, J. Photoch. Photobiol., A **179**, 330 (2006).
[19] R. E. Honrath, S. Guo, M. C. Peterson, M. P. Dziobak, J. E. Dibb, and M. A. Arsenault, J. Geophys. Res., [Atmos.] **105**, 24183, doi:10.1029/2000JD900361 (2000).
[20] C. S. Boxe, A. J. Colussi, M. R. Hoffmann, I. M. Perez, J. G. Murphy, and R. C. Cohen, J. Phys. Chem. A **110**, 3578 (2006).
[21] M. Mochida and B. J. Finlayson-Pitts, J. Phys. Chem. A **104**, 9705 (2000).
[22] E. S. N. Cotter, A. E. Jones, E. W. Wolff, and S. J.-B. Bauguitte, J. Geophys. Res. **108**, 4147, doi:10.1029/2002JD002602 (2003).
[23] D. D. Davis, J. Seelig, G. Huey, J. Crawford, G. Chen, Y. H. Wang, M. Buhr, D. Helmig, W. Neff, D. Blake, R. Arimoto, and F. Eisele, Atmos. Environ. **42**, 2831 (2008).
[24] J. R. McCabe, C. S. Boxe, A. J. Colussi, M. R. Hoffmann, and M. H. Thiemens, J. Geophys. Res., [Atmos.] **110**, D15310, doi:10.1029/2004JD005484 (2005).
[25] R. Qiu, S. A. Green, R. E. Honrath, M. C. Peterson, Y. Lu, and M. Dziobak, Atmos. Environ. **36**, 2563 (2002).
[26] F. Dominé and P. B. Shepson, Science **297**, 1506 (2002).
[27] Y. L. Yung and C. E. Miller, Science **278**, 1778 (1997).
[28] J. Erbland, W. C. Vicars, J. Savarino, S. Morin, M. M. Frey, D. Frosini, E. Vince, and J. M. F. Martins, Atmos. Chem. Phys. **13**, 6403 (2013).
[29] J. A. Schmidt, M. S. Johnson, and R. Schinke, P. Natl. Acad. Sci. U.S.A. **110**, 17691 (2013).
[30] S. A. Ndengue, F. Gatti, R. Schinke, H. D. Meyer, and R. Jost, J. Phys. Chem. A **114**, 9855 (2010).
[31] R. Jost, Adv. Quantum Chem. **55**, 75 (2008).
[32] C. Meusinger, T. A. Berhanu, J. Erbland, J. Savarino, and M. S. Johnson, J. Chem. Phys. **140**, 244305 (2014).
[33] G. Mark, H. G. Korth, H. P. Schuchmann, and C. von Sonntag, J. Photoch. Photobio., A **101**, 89 (1996).
[34] J. Erbland, W. C. Vicars, J. Savarino, S. Morin, M. M. Frey, D. Frosini, E. Vince, and J. M. F. Martins, Atmos. Chem. Phys. Discuss. **12**, 28559 (2012).
[35] J. K. Böhlke, S. J. Mroczkowski, and T. B. Coplen, Rapid Commun. Mass Spectrom. **17**, 1835 (2003).
[36] M. M. Frey, N. Brough, J. L. France, P. S. Anderson, O. Traulle, M. D. King, A. E. Jones, E. W. Wolff, and J. Savarino, Atmos. Chem. Phys. **13**, 3045 (2013).
[37] S. Morin, J. Savarino, M. M. Frey, F. Dominé, H. W. Jacobi, L. Kaleschke, and J. M. F. Martins, J. Geophys. Res., [Atmos.] **114**, D05303, doi:10.1029/2008JD010696 (2009).
[38] D. M. Sigman, K. L. Casciotti, M. Andreani, C. Barford, M. Galanter, and J. K. Bohlke, Anal. Chem. **73**, 4145 (2001).
[39] K. L. Casciotti, D. M. Sigman, M. G. Hastings, J. K. Böhlke, and A. Hilkert, Anal. Chem. **74**, 4905 (2002).
[40] J. Kaiser, M. G. Hastings, B. Z. Houlton, T. Röckmann, and D. M. Sigman, Anal. Chem. **79**, 599 (2007).
[41] G. Michalski, J. Savarino, J. K. Bohlke, and M. Thiemens, Anal. Chem. **74**, 4989 (2002).
[42] J. R. Taylor, *An Introduction to Error Analysis: The Study of Uncertainties in Physical Measurements*, 2nd ed. (University Science Books, 1997).
[43] L. Chu and C. Anastasio, J. Phys. Chem. A **107**, 9594 (2003).
[44] J. L. France, M. D. King, M. M. Frey, J. Erbland, G. Picard, S. Preunkert, A. MacArthur, and J. Savarino, Atmos. Chem. Phys. **11**, 9787 (2011).
[45] D. Madsen, J. Larsen, S. K. Jensen, S. R. Keiding, and J. Thogersen, J. Am. Chem. Soc. **125**, 15571 (2003).
[46] J. A. Schmidt, M. S. Johnson, and R. Schinke, Atmos. Chem. Phys. **11**, 8965 (2011).
[47] J. Lee-Taylor and S. Madronich, J. Geophys. Res., [Atmos.] **107**, 4796, doi:10.1029/2002JD002084 (2002).
[48] M. Erko, G. H. Findenegg, N. Cade, A. G. Michette, and O. Paris, Phys. Rev. B **84**, 104205 (2011).
[49] M. R. Waterland and M. K. Kelley, J. Chem. Phys. **113**, 6760 (2000).
[50] H. Wang, E. Borguet, and K. B. Eisenthal, J. Phys. Chem. B **102**, 4927 (1998).
[51] H. McConnell, J. Chem. Phys. **20**, 700 (1952).
[52] I. Mochida, N. Shirahama, S. Kawano, Y. Korai, A. Yasutake, M. Tanoura, S. Fujii, and M. Yoshikawa, Fuel **79**, 1713 (2000).
[53] R. Schinke, *Photodissociation Dynamics* (Cambridge University Press, Cambridge, U.K., 1993).
[54] S. Y. Grebenshchikov, Z. W. Qu, H. Zhu, and R. Schinke, Phys. Chem. Chem. Phys. **9**, 2044 (2007).
[55] A. Delon, R. Jost, and M. Lombardi, J. Chem. Phys. **95**, 5701 (1991).
[56] J. M. Flaud and R. Bacis, Spectrochim. Acta A **54**, 3 (1998).
[57] G. Picard and Q. Libois, personal communication (2013).
[58] M. Frey, personal communication (2013).